



Prediction of Functional Loss of Human Angiogenin Mutants Associated with ALS by Molecular Dynamics Simulations

Aditya K. Padhi¹, Bhyravabhotla Jayaram^{1,2,3} & James Gomes¹

¹Kusuma School of Biological Sciences, ²Department of Chemistry, ³Supercomputing Facility for Bioinformatics and Computational Biology Indian Institute of Technology Delhi Hauz Khas, New Delhi-110016, India.

SUBJECT AREAS:

PROTEIN FUNCTION
PREDICTIONS

AMYOTROPHIC LATERAL
SCLEROSIS

COMPUTATIONAL BIOPHYSICS

MOTOR NEURON DISEASE

Received
22 October 2012

Accepted
18 January 2013

Published
7 February 2013

Correspondence and
requests for materials
should be addressed to
J.G. (jgomes@
bioschool.iitd.ac.in)

Several missense mutations in the coding region of angiogenin (*ANG*) gene have been identified in Amyotrophic Lateral Sclerosis (ALS) patients. These mutations lead to loss of either ribonucleolytic activity or nuclear translocation activity or both of *ANG* (protein encoded by *ANG* gene) causing ALS. We present here a cohesive and comprehensive picture of the molecular origins of functional loss of all ALS associated *ANG* mutants, emerging via extensive molecular dynamics simulations. Our method effectively predicts that conformational change of His114 results in loss of ribonucleolytic activity and that reduction of solvent accessible surface area of nuclear localization signal residues ³¹RRR³³ results in loss of nuclear translocation activity. These predictions hold true, without exception, for all *ANG* mutants studied and can be employed to infer whether a new *ANG* mutation is causative of ALS or benign ahead of experimental findings.

Amyotrophic Lateral Sclerosis (ALS, OMIM #105400) is a fatal progressive neurodegenerative disorder affecting upper and lower motor neurons (MNs). It is characterized by the selective loss of MNs in the motor cortex, brain stem and spinal cord, consequently leading to paralysis and death, usually between 3–5 years of diagnosis^{1,2}. Most of the ALS cases are sporadic with no knowledge of its cause while ~10% of them are familial. The etiology and mechanisms underlying this debilitating disease are poorly understood. There is no primary therapy for this disorder at present, and the only available drug for treatment is an antiglutamatergic compound, riluzole, which merely extends lifespan by a few months but has no crucial effect on improving the symptoms. As most of the ALS cases are sporadic, there is a need to understand the underlying mechanisms, which may lead to the development of a successful therapy. Genetic factors have emerged as one of the key causes contributing to ALS etiology. An increasing number of ALS associated genes have been identified recently. Until now, mutations in the *SOD1* gene were reported to be one of the major known causes of ALS¹. *SOD1* mutations are found in both sporadic and familial ALS patients and studied in great detail. Recently, mutations in several other genes including *FUS/TLS*, *VAPB*, *ANG*, *TARDBP*, *FIG4* and a hexanucleotide-repeat expansion (GGGGCC) in the *C9ORF72* have been identified to be the causative genetic factors of adult onset of ALS^{1,3}. Other risk factors have also been identified, through genetic association studies, which include deletions or insertions in the neurofilament heavy chain gene, heterochromatin gene (*HFE*) and paraoxonase-1 (*PONI*) in ALS^{1–4}.

Since the first report of Greenway et al.⁵, *ANG* has emerged as one of the key genes in ALS. *ANG* encodes the angiogenin protein (*ANG*), a 14.1 kDa polypeptide, which induces neovascularization⁶ and has 33% sequence identity with bovine pancreatic RNase A. *ANG* is angiogenic due to the presence of two functional sites such as the receptor-binding site (⁶⁰NKNGNPHREN⁶⁸) and the nuclear localization signal (²⁹IMRRRGL³⁵) using which it binds to its target cells and undergoes nuclear translocation respectively; the residues His13, Lys40 and His114 serve as the catalytic triad for ribonucleolytic activity^{6,7}. The three functional sites of *ANG* are presented in Figure 1. It has been shown that wild-type *ANG* (WT-*ANG*) has a wide tissue distribution and is strongly expressed in both endothelial cells, and MNs in fetal and adult spinal cord of humans⁸. WT-*ANG* acts as a neuroprotective factor because it determines the physiology and health of MNs by inducing angiogenesis, stimulating neurite outgrowth and path-finding and protecting MNs from hypoxia-induced death^{8,9}. Several reports on heterozygous missense mutations of *ANG* and consequent experimental functional assays have shown that *ANG* insufficiency and loss-of-functions due to these mutations lead to ALS pathogenesis. Functional assay experiments carried out by Wu et al.⁸ showed that three mutants (K17I, S28N, P112L) identified from North American ALS patients are associated with loss of angiogenic activity and concluded that loss of either ribonucleolytic activity or nuclear translocation activity or both ensue in the loss of angiogenic function, which in turn stimulates ALS. Crabtree et al.¹⁰ performed the

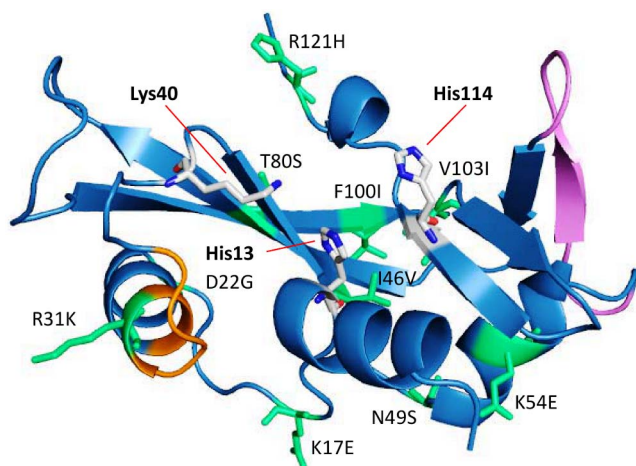


Figure 1 | Cartoon representation of human angiogenin showing its functional sites and missense mutations found in ALS patients. All the reported ALS associated angiogenin (PDB ID: 1B1I) mutations are labeled and represented as stick model (lime green color). The three key functional sites of human angiogenin (nuclear localization signal, receptor binding site and catalytic triad) are also shown. Angiogenin protein: sky blue color, nuclear localization signal: orange color, receptor binding site: violet color and catalytic triad of angiogenin: blue and grey stick models.

ribonucleolysis assay of seven ANG mutants identified from Irish and Scottish ALS patients and showed that these mutants lost their ribonucleolytic activity. These results demonstrated that compromised angiogenic activity due to missense mutations is associated with ALS pathogenesis and progression.

We carried out earlier a preliminary study using molecular dynamics (MD) simulations to understand functional loss mechanisms of certain ANG mutants and their correlation with ALS⁷. We followed this up with a comprehensive analysis of all known mutants. While this manuscript is being prepared, an experimental study on 11 ALS associated ANG mutants was reported¹¹, which corroborates our findings and offers an opportunity to critically assess the molecular dynamics based strategy to decipher the role of missense mutations.

In this report, we present results of a series of MD simulations, and infer the functional loss mechanisms of all known ALS associated ANG mutants listed in Table 1. Mutations located proximal to or located at the catalytic triad with their obvious role in loss of ribonucleolytic activity and those present in the signal peptide region are however not considered in this study. The sites of mutations of all the ANG mutants studied are presented in Figure 1. We find that the loss of ribonucleolytic activity in ALS associated ANG mutants is due to a characteristic conformational change of catalytic residue His114 and loss of nuclear translocation activity is due to local folding, and hence decrease in solvent accessible surface area (SASA), of nuclear localization signal residues ³¹RRR³³. The close match between simulation results and reported experimental data establishes the strength of this method and its application as a predictive tool to determine if an ANG mutation is deleterious or benign, and if deleterious, the probable mechanism of its loss-of-functions.

Results

Functional evaluation of ANG mutants. *Ribonucleolytic activity of ANG mutants.* The ribonucleolytic activity of ANG is governed by the catalytic triad comprising residues His13, Lys40 and His114. To investigate the structural and dynamic changes of the catalytic

Table 1 | Detailed list of human angiogenin mutations reported in ALS patients with their corresponding loss-of-functions data from reported experiments and our MD simulations

Human ANG mutation	Experimental findings from literatures		MD simulation results		Remarks	Reference
	Ribonucleolytic activity	Nuclear translocation activity	Ribonucleolytic activity	Nuclear translocation activity		
K17I#	Loss ^{8,10,11}	No loss ^{8,11}	Loss ⁷	No loss ⁷		31–35
S28N#	Loss ^{8,11}	Loss ^{8,11}	Loss ⁷	Loss ⁷		8
P112I#	Partial loss ^{8,11}	Loss ^{8,11}	Partial loss ⁷	Loss ⁷		8
I46V	Partial loss ^{10,11}	No loss ¹¹	Partial loss	No loss		31, 32, 35–39
K17E	Partial loss ^{10,11}	No loss ¹¹	Partial loss	No loss		31
R31K	Minor loss ^{10,11}	No loss ^{10,11}	Minor loss	No loss		31
V103I	Not reported	Not reported	No loss	Loss		40
D22G	Not reported	Not reported	Loss	No loss		41
V113I#	Minor loss ¹¹	Transient activity ¹¹	No loss ⁷	Loss ⁷		37
Q12L*	Loss ^{10,11}	No loss ¹¹			*Located near His13	31
C39W*	Loss ^{10,11}	Not reported			*Located near Lys40	31
K40I*	Loss ^{10,11}	No loss ¹¹			*Mutation of Lys40	31, 5
H114R*	Loss ¹¹	No loss ¹¹			*Mutation of His114	37
F-13S*	Not reported	Not reported			*Not located in mature ANG	37, 38
F-13L*	Not reported	Not reported			*Not located in mature ANG	35
M-24I*	Not reported	Not reported			*Not located in mature ANG	37, 38
P-4S*	Not reported	Not reported			*Not located in mature ANG	37, 8
R121C	Not reported	Not reported	No loss	No loss	SOD1-G93D patient with R121C-ANG mutation	23
R121H	No loss ¹¹	Transient activity ¹¹	No loss	Loss		36
K54E	No loss ¹¹	Not reported	No loss	Loss		35
T80S	Not reported	Not reported	Loss	No loss		32, 44
F100I	Not reported	Not reported	No loss	Loss		32, 44
N49S	Not reported	Not reported	Minor loss	No loss		42
L35P#	Not reported	Not reported	Loss ⁷	Loss ⁷		43
K60E#	Not reported	Not reported	No loss ⁷	No loss ⁷		43

#ANG mutants for which simulation results are presented in reference 7.



residues in ALS associated ANG mutants, we have visualized the catalytic triad using VMD¹². It was observed that the conformation of catalytic residue His114 changed significantly in I46V, K17E, R31K, D22G, N49S and T80S ANG mutants. It was noticed that this conformational change was most severe in case of D22G mutant followed by T80S, I46V, K17E, R31K and N49S mutants. Snapshots of mutants showing conformational change of the catalytic residue His114 are presented in Figure 2. Two snapshots per mutant (one at 0 ns and another at 25 ns of the molecular dynamics trajectories) for which there is a conformational change of His114 are presented in Figure 2a. Similarly, in Figure 2b, two snapshots at 0 ns and 25 ns are displayed for the mutants, which do not show any conformational change of His114. The change in conformation of His114 was computed quantitatively and the

HA-CA-CB-CG dihedral angle change of His114 was determined for all the ANG mutants (Figure 3). We observed a change in dihedral angle from the mean -80° position (for WT-ANG) to -179° for the mutants I46V, K17E, R31K, D22G, T80S and N49S and none for V103I, K54E, F100I, R121C and R121H (Figures 3a and 3b).

We examined the frequency of conformational switching of His114 over all the frames of MD simulation for each of the mutants and compared these with the WT-ANG frequency (Figure 4). We observed that the mutants I46V, K17E and R31K, for which the loss of ribonucleolytic activity has been experimentally verified¹⁰, the conformational frequency of His114 between -80° to -100° is much lower than that for WT-ANG. There is a simultaneous increase in conformational frequency shift in dihedral angle between -160° to -180° . Likewise, for the mutants K54E and R121H, we observed

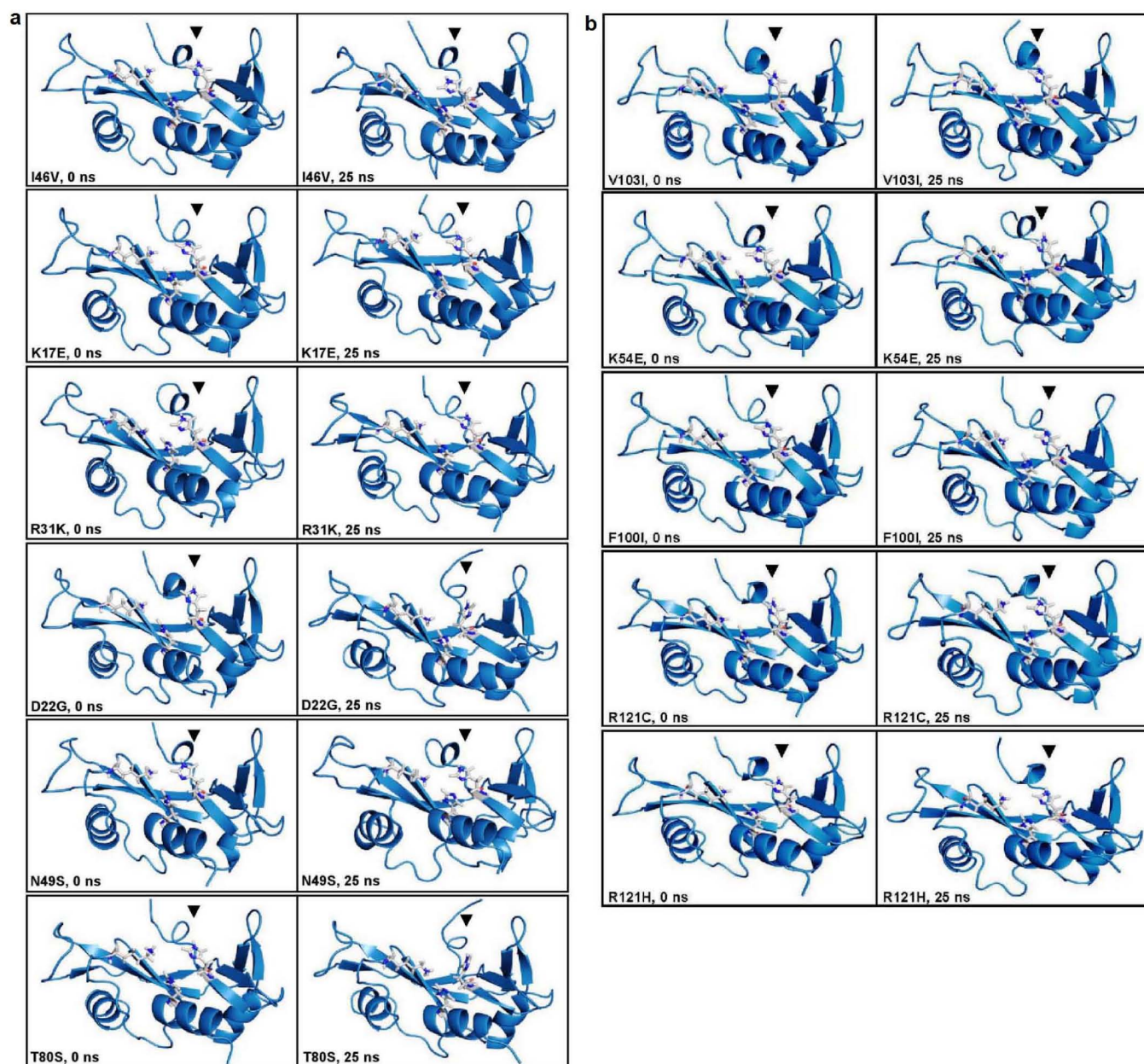


Figure 2 | Conformational change of His114 in ALS associated ANG mutants. (a) Observed conformational change of catalytic residue His114 during MD simulations of ALS associated ANG mutants (I46V, K17E, R31K, D22G, N49S and T80S) is presented. Time 0 ns represents the start of production phase after equilibration and 25 ns represents the end of production phase. (b) Observed stable and native conformation of catalytic residue His114 during MD simulations of certain ALS associated ANG mutants (V103I, K54E, F100I, R121C and R121H) is presented. Time 0 ns represents the start of production phase after equilibration and 25 ns represents the end of production phase.

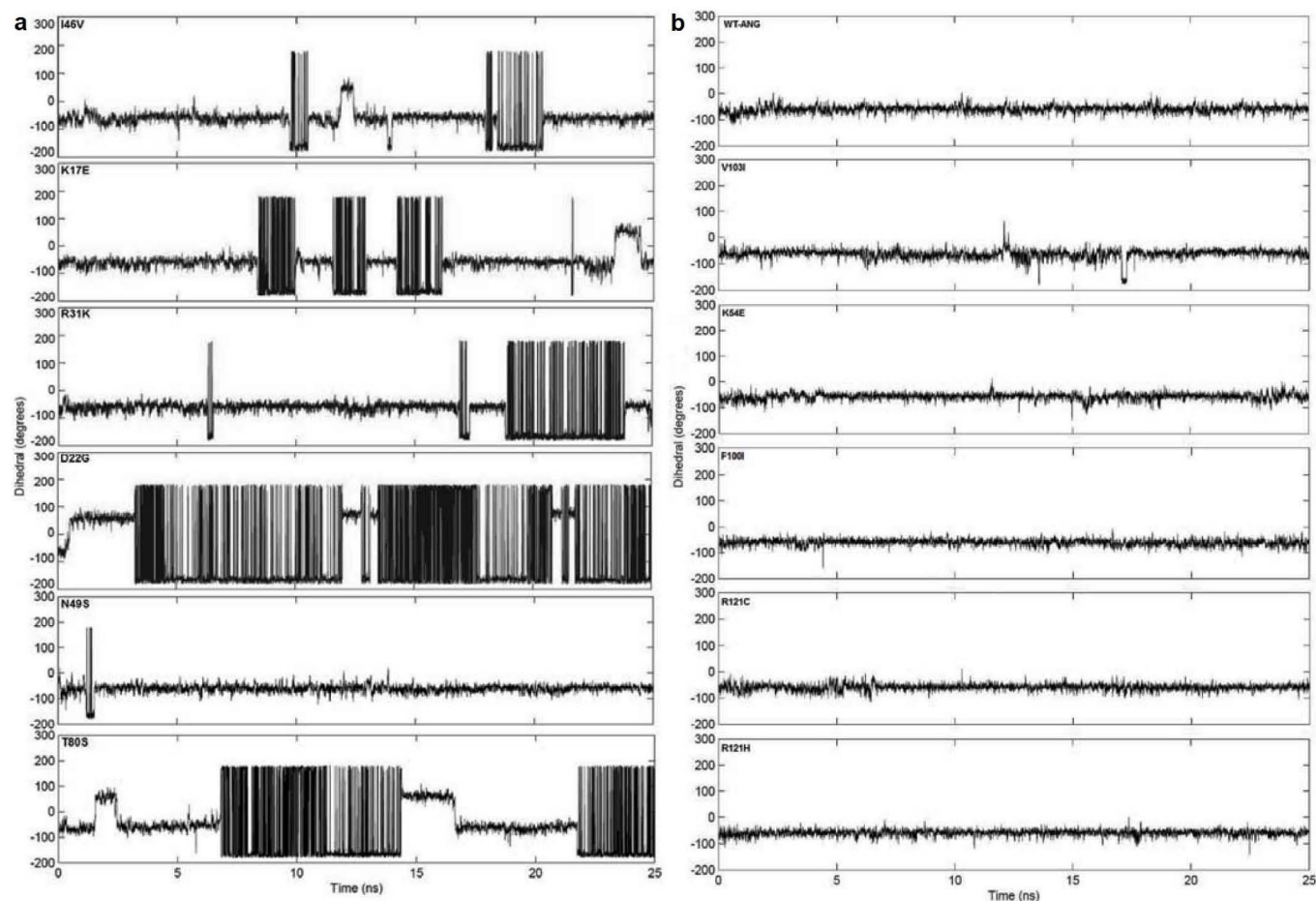


Figure 3 | HA-CA-CB-CG dihedral angle change of His114 from MD simulations of ALS associated ANG mutants. (a) Computed change in HA-CA-CB-CG dihedral angle of catalytic residue His114 from MD simulation as a function of time. ANG mutants (I46V, K17E, R31K, D22G, N49S and T80S) exhibited change in dihedral angle of His114 and subsequently loss of ribonucleolytic activity. (b) Computed change in HA-CA-CB-CG dihedral angle of catalytic residue His114 from MD simulation as a function of time for WT-ANG and mutants V103I, K54E, F100I, R121C and R121H. Stable dihedral angle of His114 throughout simulations for these mutants suggests no loss of ribonucleolytic activity.

that conformational frequency of His114 was between -80° to -100° , similar to WT-ANG (Figure 4).

We further observed that mutations distal to the functional sites of ANG influenced the conformation of His114 through a conserved hydrogen bond interaction path. The conserved path was determined by tracing hydrogen bond interactions between the mutational site and His114 using a bond length cut-off ≤ 3.2 Å, averaged over individual MD trajectories of the mutants. The hydrogen bond interactions were computed using UCSF CHIMERA package¹³ and visualized using Cytoscape¹⁴. For mutants I46V, K17E, R31K, D22G, N49S and T80S, we found the shortest paths from the mutational sites Val46, Glu17, Lys17, Gly22, Ser49 and Ser80 respectively (Figure 5). However, in case of mutants K54E, F100I, R121C and R121H, no hydrogen bond interaction path from the site of mutation to His114 were identified. In the case of V103I, a different shortest hydrogen bond connecting path from Ile103 to His114 was identified (Figure 6). In all the connecting paths for the mutants showing conformational change of His114, we noticed that the percentage hydrogen bond occupancy between residues His114-Ala106 and Ala106-Val113 increased significantly compared to mutants retaining ribonucleolytic activity.

Previous experimental results showed that Leu115 is a key residue responsible for weak ribonucleolytic activity while Thr44 helps in substrate recognition¹⁵. In the case of D22G mutant, which exhibited severe conformational change in His114, the path passes through only Leu115. However, for mutants I46V, K17E and R31K which

retained partial ribonucleolytic activity¹⁰, the hydrogen bond interaction path from the site of mutation to His114 passed through both Leu115 and Thr44, and even for N49S which exhibited the shortest duration of conformational change in His114. A different hydrogen bond interaction path was observed for T80S, passing directly between Ser80 and Thr44 leading to His114 (Figure 5). The percentage hydrogen bond occupancy values between Thr44-Thr80 and Asp116-Ser118 pair of residues, known to be important factors for weak ribonucleolytic activity¹⁵, were calculated from the MD trajectories of WT-ANG and the mutants and presented in Supplementary Table S1.

Docking analysis to ascertain loss of ribonucleolytic activity. From our simulation results, we found that the catalytic residue His114 of mutants I46V, K17E, R31K, D22G, T80S and N49S changed its conformation from WT-ANG native state but it did not for mutants V103I, K54E, F100I, R121C and R121H (Figures 3a and 3b). To correlate this change in conformation of catalytic residue His114 with loss of ribonucleolytic activity in certain mutants, docking simulations were performed using ParDOCK^{16–19}. NCI-65828, which is an inhibitor of ribonucleolytic activity of ANG, was used for docking of mutant ANG proteins²⁰. Snapshots of ANG mutants were captured at both native and altered His114 conformations from MD trajectory and docked against NCI-65828. It was found that the binding free energies averaged over the respective trajectories were significantly lower for the mutants exhibiting conformational

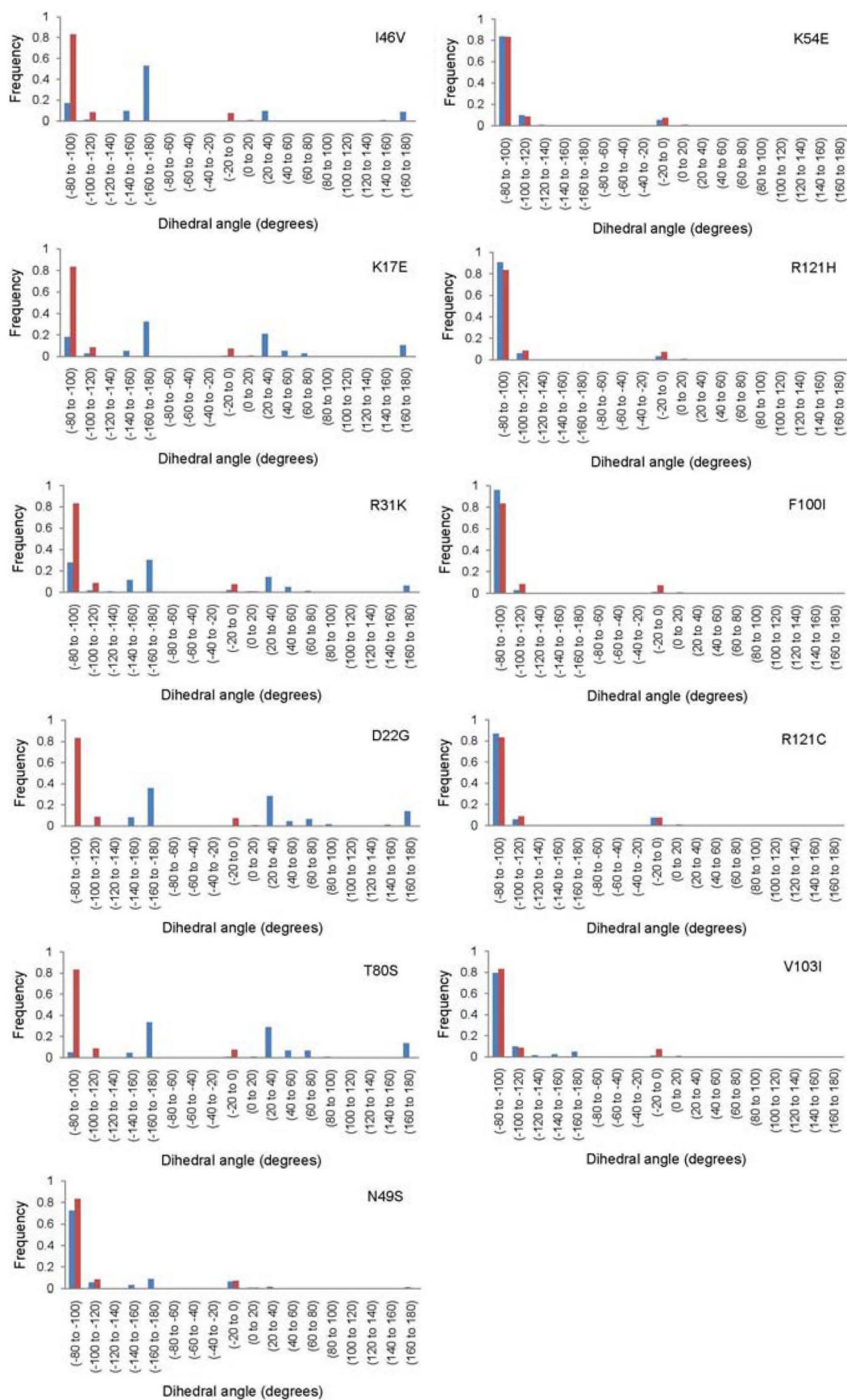


Figure 4 | Frequency of characteristic conformational change in His114 dihedral angle. The frequency of conformational change of His114 for all the ANG mutants is presented. The panels show a comparison of the frequency of conformational change in His114 dihedral angle of WT-ANG (red bars) with ANG mutants (blue bars).

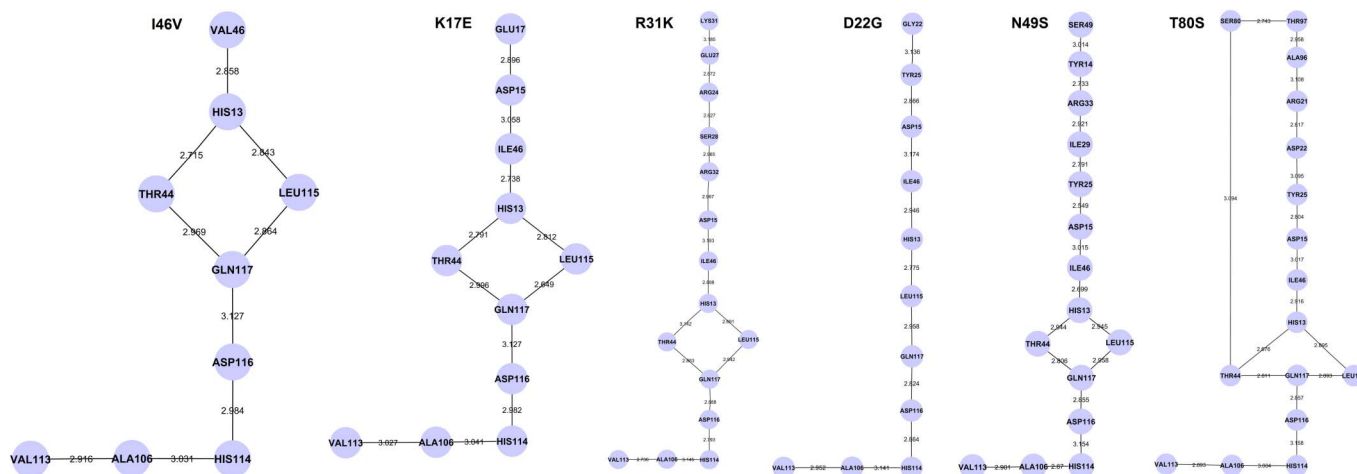


Figure 5 | Identified hydrogen bond interaction paths from the site of mutation to His114 in ANG mutants. Observed hydrogen bond interaction paths from the site of mutation to catalytic residue His114 are presented for I46V, K17E, R31K, D22G, N49S and T80S angiogenin mutants. The node represents the amino acid residue linked through hydrogen bond and edge represents the bond length between them. Simulation results show that these hydrogen bond interaction paths are conserved and hence induces loss of ribonucleolytic activity in ANG mutants.

switching of His114 compared to WT-ANG and mutants retaining the native His114 conformation. The computed binding free energy averaged over the simulation of each docked conformation is presented in Supplementary Table S2.

Nuclear translocation activity of ANG mutants. The loss of nuclear translocation activity of ANG mutants was investigated by computing the SASA. The SASA of the nuclear localization signal residues (³¹RRR³³) was calculated as these residues are located on the protein surface and largely accessible to solvent. As the ³¹RRR³³ have been known to play a significant role in nuclear translocation activity^{21,22}, SASA were calculated for all ANG mutants from their respective MD trajectories. It was found that WT-ANG and mutants I46V, K17E, R31K, D22G, N49S, T80S and R121C have higher SASA values compared to mutants V103I, K54E, F100I and R121H (Figures 7a and 7b).

Discussion

Loss of ribonucleolytic activity or nuclear translocation activity or both are correlated with ALS in patients with certain ANG mutations⁷. We asked if the conformational switching of His114, the conserved hydrogen bond interaction path and the reduction of SASA in ANG mutants were global attributes that could be used to predict if new mutations were deleterious. We carried out MD simulations to determine which of the known mutations caused conformational switching of catalytic residue His114 and folding of nuclear localization signal residues ³¹RRR³³.

We first consider the predictions of loss (or not) of ribonucleolytic activity of ANG mutants. Simulation results showed that the His114 residue in I46V, K17E, R31K, D22G, N49S and T80S ANG mutants, acquired the altered conformation of -179° (Figure 2a) measured quantitatively by HA-CA-CB-CG dihedral angle (Figure 3a). Mutants I46V, K17E and R31K, for which a partial loss of ribonucleolytic activity was reported¹⁰, exhibited change in conformation of His114 over shorter durations. We calculated the shift in conformational frequency of His114 over the 25 ns period and observed that these mutants showed a distinctly lower frequency compared to WT-ANG between -80° and -100° dihedral angle. These mutants also show conformational frequency between -160° and -180° , and between 160° and 180° , which are absent in WT-ANG. These observations correlate with VMD visualizations of His114 conformational switching (Figure 4). Crabtree et al.¹⁰ also reported that R31K mutant

showed no appreciable loss of ribonucleolytic activity and yet was associated with ALS. The conformational frequency analysis carried out by us shows that this mutant would exhibit only partial loss of ribonucleolytic activity. We observed a significant conformational change in His114 dihedral angle during VMD visualization for mutants D22G and T80S, whereas, the observed change was not significant for N49S mutant. Hence, the N49S mutant may be linked to ALS by a minor loss of ribonucleolytic activity (Figures 2a, 3a and 4). The other ANG mutants V103I, K54E, F100I, R121C and R121H did not exhibit any conformational change of His114 (Figures 2b and 3b) and exhibited conformational frequencies similar to WT-ANG (Figure 4), suggesting these mutations may not cause loss of ribonucleolytic activity. We also observed that the conformational frequency of His114 for mutant R121H between -80° and -100° dihedral angle was higher than WT-ANG, indicating that this mutant may possess a higher ribonucleolytic activity¹¹. Overall, our predictions for the loss of ribonucleolytic activity of ANG mutants correlate well with reported experimental results.

It is interesting to note that most ANG mutations identified in ALS patients are structurally remote from the functional sites except a few which are mutations of the catalytic triad residues (Table 1). This emphasizes the significance and importance of molecular dynamics simulations method reported here, for probing the underlying molecular mechanisms. The functional consequences of those mutants where the mutational residues are distal to the functional sites but still disease associated were examined. We found that mutants I46V, K17E and R31K, which retain partial ribonucleolytic activity, possess hydrogen bond interaction paths that mediate through both Thr44 and Leu115 (Figure 5). Similar paths were observed for N49S. However, for D22G, which exhibited a strong conformational change in His114, a single path through Leu115 was identified (Figure 5). The T80S mutant has two hydrogen bond interaction paths - the first traverses through Leu115 and the second connects the point of mutation Ser80 directly to Thr44 and influences His114 through a short-circuited path Ser80-Thr44-Gln117-Asp116-His114. The short path through Ser80 may be responsible for stronger conformational changes in His114 for T80S (Figure 5). No hydrogen bond interaction paths were observed for the other ANG mutants K54E, F100I, R121C and R121H. However, for V103I, which does not show any conformational switching of His114, a different hydrogen bond path not mediated through Thr44 was observed (Figure 6). This shows that hydrogen bond interaction path from

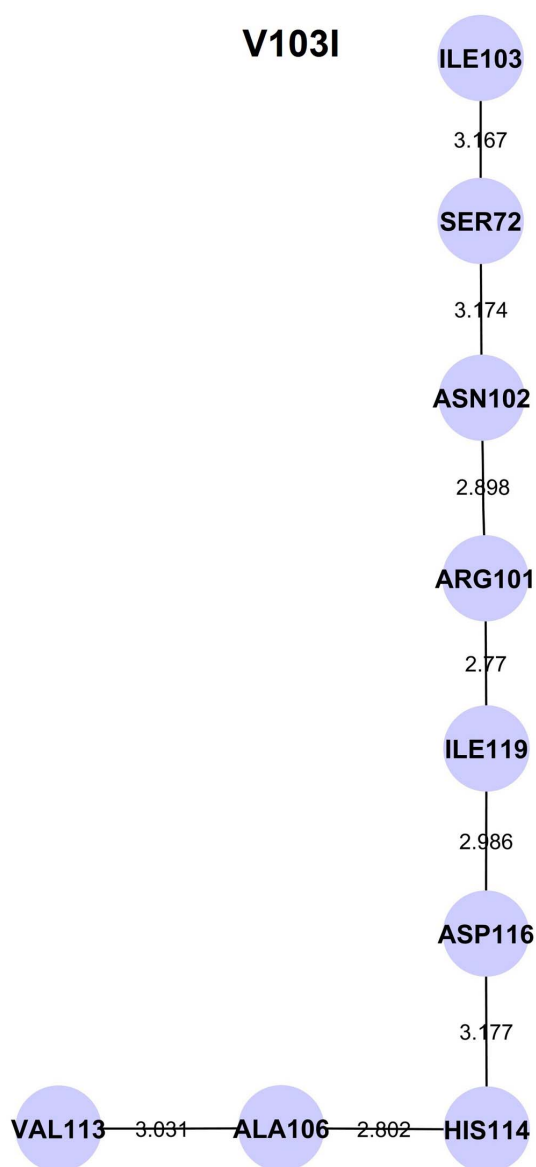


Figure 6 | Identified hydrogen bond interaction path from the site of mutation Ile103 to His114 in V103I mutant. The observed hydrogen bond interaction path from the site of mutation Ile103 to catalytic residue His114 is shown. The amino acid residues represented by the nodes are linked through hydrogen bonds. The numerical values shown on the edges are the hydrogen bond lengths. That is a different hydrogen bond interaction path, neither mediated through Leu115 nor through Thr44 and it is not crucial to the loss of ribonucleolytic activity.

the site of mutation to His114 is a crucial and useful parameter that could distinguish between mutations that cause a loss of ribonucleolytic activity from those that do not.

To confirm that the conformational change of His114 results in loss of ribonucleolytic activity in certain ANG mutants, molecular docking of the mutant ANG protein with NCI-65828, a known inhibitor of ribonucleolytic activity, was performed. The average binding energies calculated were distinctly lower for mutants with altered His114 conformation (Supplementary Table S2) compared to WT-ANG and mutants retaining native His114 conformation.

We now consider the loss of nuclear translocation activity of ANG mutants in relation to reported ALS pathogenesis. We observed that the SASA values of WT-ANG and mutants I46V, K17E, R31K, D22G, N49S, T80S and R121C were very high compared to mutants

V103I, K54E, F100I and R121H (Figures 7a and 7b). Based on this demarcation, we predict that I46V, K17E, R31K, D22G, N49S, T80S and R121C would retain their nuclear translocation activity while V103I, K54E, F100I and R121H would exhibit loss of it. Our predictions for I46V, K17E, R31K and R121H were found to be in agreement with recently reported experimental results¹¹. It is interesting to note that our method correctly predicts no loss in nuclear translocation activity for R31K mutant, which embeds an altered nuclear translocation sequence ³¹KRR³³ (Figure 7a). Crabtree et al.¹⁰ have previously discussed that like arginine, lysine can also function in nuclear translocation sequences. Further, it has been seen that in bovine, pig, mouse, and rabbit, ANG contains lysine instead of arginine and retains its nuclear translocation activity. Our simulation results indicate that R31K mutant is ALS pathogenic possibly due to loss of ribonucleolytic activity and not due to loss of nuclear translocation activity.

An interesting case was observed for R121C missense mutation in ANG. Although previous reports show that ALS patients with SOD1-G93D mutation exhibit slow disease progression, an Italian patient bearing an additional ANG-R121C mutation, died after 30 months of symptom onset²³. This gave the impression that ANG-R121C mutation may have accelerated the disease progression. However, our simulation results show that R121C-ANG mutant did not exhibit any loss-of-functions (ribonucleolytic activity and nuclear translocation activity), suggesting some unknown mechanism possibly enhanced the rapid disease progression.

We have established through this work that conformational switching of His114, presence of the conserved hydrogen bond interaction path mediated through Leu115 and reduction of SASA of nuclear localization signal residues ³¹RRR³³ in ANG mutants are global attributes that distinguish deleterious from benign mutations. Using these attributes we predicted the functional loss mechanisms of known ANG mutants. We have also made prediction on how mutants, for which experimental data has not yet been reported, are ALS associated. By our method, mutants D22G, T80S and N49S exhibited loss of ribonucleolytic activity and mutants F100I and V103I exhibited loss of nuclear translocation activity. The static picture of mutant proteins obtained by modeling the mutation followed by energy minimization does not yield a satisfactory explanation about the molecular mechanisms. We have shown how our method based on time evolution studies of MD simulations gives insights into the molecular mechanisms of mutations causing disease. With this computational protocol, the functional loss mechanisms of newly identified ANG mutations and their association with ALS can be predicted ahead of experimental findings. Creation of a predictive tool for ANG mutations based on these global attributes will help clinicians to understand ALS pathogenesis and progression. Further studies are in progress to understand functional implications of ANG mutations using accelerated molecular dynamics simulations.

Methods

Preparation of starting structures and MD simulations. The X-ray crystal structure of human angiogenin¹⁵ obtained from Protein Data Bank (PDB code: 1B11) was used as the starting structure for MD simulations. Heteroatoms, crystallographic waters and cofactor, CIT were removed from the structure prior to simulation. The starting structures of the mutants were modeled *in silico* by mutating the target residues with the desired amino acids keeping the secondary structure intact. Hydrogen atoms were added using the Xleap tool of Amber 10²⁴. The system was subsequently solvated with TIP3P water in an octahedral box with ~10 Å between the protein surface and the box boundary²⁵. Each of the systems was electrostatically neutralized by the addition of Cl⁻ counter ions. The SANDER module of AMBER 10 package with the "ff99SB" force field was used for all MD simulations²⁶.

The MD simulations were carried out for 25 ns for all the ALS associated ANG mutants except Q12L, C39W, K40I, H114R, F-13S, F-13L, M-24I and P-4S (Table 1). MD simulations of Q12L, C39W, K40I and H114R mutants were not performed because the mutational sites were close to or located at the catalytic site. C39W mutation eliminates its disulphide bridge with C92 and consequently loses its ribonucleolytic activity¹⁰. The other three mutants (P-4S, F-13L, F-13S and M-24I)

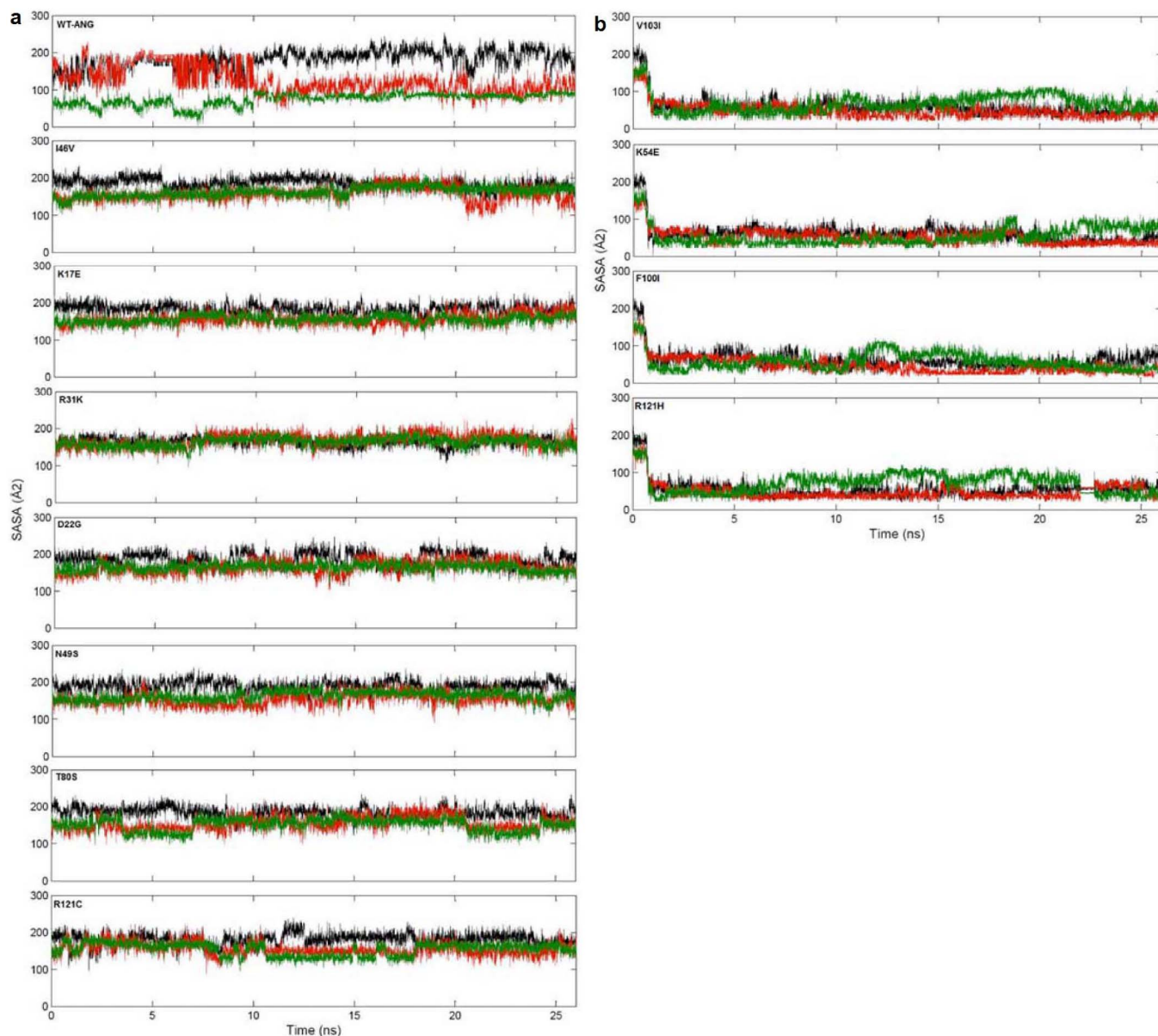


Figure 7 | Computed solvent accessible surface area of $^{31}\text{RRR}^{33}$ from MD simulations. (a) Computed solvent accessible surface area from MD simulations of nuclear localization signal residues $^{31}\text{RRR}^{33}$ for WT-ANG and I46V, K17E, R31K, D22G, N49S, T80S and R121C angiogenin mutants. Solvent accessible surface area of $^{31}\text{RRR}^{33}$ is represented as R31: black, R32: red and R33: green colored lines. SASA was calculated starting from the energy minimized structure. (b) Computed solvent accessible surface area from MD simulations of nuclear localization signal residues $^{31}\text{RRR}^{33}$ for V103I, K54E, F100I and R121H angiogenin mutants. Solvent accessible surface area of $^{31}\text{RRR}^{33}$ is represented as R31: black, R32: red and R33: green colored lines. SASA was calculated starting from the energy minimized structure.

are not located in the mature protein because they are present in the signal peptide region of ANG.

Each simulation was performed for 25 ns in the isothermal isobaric ensemble (NPT). For each system, the standard simulation protocol was followed as reported in our previous article⁷. Each system was energy minimized for 2500 steps of steepest descent followed by 1000 steps conjugate gradient minimization to eliminate close van der Waals contacts and then gradually heated from 0 to 300 K in 200 ps followed by constant temperature equilibration at 300 K for 1000 ps. Following this, 25 ns production MD runs were carried out with periodic boundary conditions in the NPT ensemble, at a temperature of 300 K with Berendsen temperature coupling and a constant pressure of 1 atm with isotropic molecule-based scaling²⁷. Bond lengths involving bonds to hydrogen(s) were constrained using SHAKE algorithm²⁸. Long-range electrostatic forces were calculated using the particle-mesh Ewald (PME) method²⁹. The energy stabilization and the root mean square deviations (RMSD) of the protein were analyzed by sampling the coordinates of the trajectory at every 1 ps. The analyses of MD simulations were carried out by PTRAJ module of AMBER 10. MD simulations were performed on a 320 processor SUN Microsystems cluster at the Supercomputing Facility (<http://www.scfbio-iitd.res.in>) of Indian Institute of Technology Delhi.

MD simulation protocol has been validated based on the crystal structure of WT-ANG. Also, several parameters and methodology were evaluated to validate the MD protocol. The root mean square deviation (RMSD) values were monitored for WT-ANG and each of the ANG mutants (I46V, K17E, R31K, D22G, N49S, T80S, V103I, K54E, F100I, R121C and R121H) from 25 ns simulation trajectory (see supplementary Figure S1). The RMSD of each mutant was compared with the computed RMSD of the WT-ANG and other mutants. It was found that the RMSD data of all the mutants behaved similarly to WT-ANG RMSD profile. We noticed that ANG mutants I46V and T80S have marginally higher RMSD profiles compared to all other ANG mutants while V103I had a higher RMSD at around 10 ns and stabilized thereafter (see supplementary Figure S1).

Docking of NCI-65828 with ANG. The loss of ribonucleolytic activity for the ANG mutants was studied using ParDOCK, which is an all atom energy based Monte Carlo docking protocol^{16–19}. We have retrieved structures of docked complex for every nanosecond from the simulation. The binding free energy was calculated for each docked complex consisting of the mutant and the known inhibitor (NCI-65828) of ribonucleolytic activity of ANG and averaged over all the structures. ParDOCK requires a reference complex (target protein bound to a reference ligand) and a



candidate molecule along with a specific mention of the centre of mass of the cavity on which the ligand is to be docked. The Active Site Prediction server (<http://www.scfbio-iitd.res.in/dock/ActiveSite.jsp>) was used for the prediction of active sites, which computes cavities (potential binding sites) in the protein. The cavity that lies in closest proximity to His114 was used for docking the compound NCI-65828.

SASA calculation of nuclear localization signal residues³¹RRR³³. SASA of nuclear localization signal residues³¹RRR³³, was calculated using MolSpace (previously called SurfVol) (<http://www.compbiochem.org/Software/molSpace/Home.html>), a Plug-in for Visual Molecular Dynamics (VMD) software (version 1.9.1)¹². SASA was calculated for all the ANG mutants using a probe radius of 1.4 Å.

Graphics. All figures were generated using the PyMOL (<http://www.pymol.org>)³⁰. Hydrogen bond interaction network figures were generated using Cytoscape (<http://www.cytoscape.org/>)¹⁴.

- Ferraiuolo, L., Kirby, J., Grierson, A. J., Sendtner, M. & Shaw, P. J. Molecular pathways of motor neuron injury in amyotrophic lateral sclerosis. *Nat Rev Neurol* **7**, 616–630 (2011).
- Hardiman, O., van den, B. E. L. & Kiernan, M. C. Clinical diagnosis and management of amyotrophic lateral sclerosis. *Nat Rev Neurol* **7**, 639–649 (2011).
- Andersen, P. M. & Al-Chalabi, A. Clinical genetics of amyotrophic lateral sclerosis: what do we really know? *Nat Rev Neurol* **7**, 603–615 (2011).
- Perry, J. J., Shin, D. S. & Tainer, J. A. Amyotrophic lateral sclerosis. *Adv Exp Med Biol* **685**, 9–20 (2010).
- Greenway, M. J. *et al.* A novel candidate region for ALS on chromosome 14q11.2. *Neurology* **63**, 1936–1938 (2004).
- Kishikawa, H., Wu, D. & Hu, G. F. Targeting angiogenin in therapy of amyotrophic lateral sclerosis. *Expert Opin Ther Targets* **12**, 1229–1242 (2008).
- Padhi, A. K., Kumar, H., Vasalkar, S. V., Jayaram, B. & Gomes, J. Mechanisms of loss of functions of human angiogenin variants implicated in amyotrophic lateral sclerosis. *PLoS One* **7**, e32479 (2012).
- Wu, D. *et al.* Angiogenin loss-of-function mutations in amyotrophic lateral sclerosis. *Ann Neurol* **62**, 609–617 (2007).
- Subramanian, V., Crabtree, B. & Acharya, K. R. Human angiogenin is a neuroprotective factor and amyotrophic lateral sclerosis associated angiogenin variants affect neurite extension/pathfinding and survival of motor neurons. *Hum Mol Genet* **17**, 130–149 (2008).
- Crabtree, B. *et al.* Characterization of human angiogenin variants implicated in amyotrophic lateral sclerosis. *Biochemistry* **46**, 11810–11818 (2007).
- Thiyagarajan, N., Ferguson, R., Subramanian, V. & Acharya, K. R. Structural and molecular insights into the mechanism of action of human angiogenin-ALS variants in neurons. *Nat Commun* **3**, 1121 (2012).
- Humphrey, W., Dalke, A. & Schulten, K. VMD: visual molecular dynamics. *J Mol Graph* **14**, 33–8, 27–8 (1996).
- Pettersen, E. F. *et al.* UCSF Chimera—a visualization system for exploratory research and analysis. *J Comput Chem* **25**, 1605–1612 (2004).
- Shannon, P. *et al.* Cytoscape: a software environment for integrated models of biomolecular interaction networks. *Genome Res* **13**, 2498–2504 (2003).
- Leonidas, D. D. *et al.* Refined crystal structures of native human angiogenin and two active site variants: implications for the unique functional properties of an enzyme involved in neovascularisation during tumour growth. *J Mol Biol* **285**, 1209–1233 (1999).
- Gupta, A., Gandhimathi, A., Sharma, P. & Jayaram, B. ParDOCK: an all atom energy based Monte Carlo docking protocol for protein-ligand complexes. *Protein Pept Lett* **14**, 632–646 (2007).
- Jain, T. & Jayaram, B. An all atom energy based computational protocol for predicting binding affinities of protein-ligand complexes. *FEBS Lett* **579**, 6659–6666 (2005).
- Singh, T., Biswas, D. & Jayaram, B. AADS—an automated active site identification, docking, and scoring protocol for protein targets based on physicochemical descriptors. *J Chem Inf Model* **51**, 2515–2527 (2011).
- Jayaram, B. *et al.* Sanjeevini: a freely accessible web-server for target directed lead molecule discovery. *BMC Bioinformatics* **13 Suppl** **17**, S7 (2012).
- Jenkins, J. L. & Shapiro, R. Identification of small-molecule inhibitors of human angiogenin and characterization of their binding interactions guided by computational docking. *Biochemistry* **42**, 6674–6687 (2003).
- Moroianu, J. & Riordan, J. F. Nuclear translocation of angiogenin in proliferating endothelial cells is essential to its angiogenic activity. *Proc Natl Acad Sci U S A* **91**, 1677–1681 (1994).
- Moroianu, J. & Riordan, J. F. Identification of the nucleolar targeting signal of human angiogenin. *Biochem Biophys Res Commun* **203**, 1765–1772 (1994).
- Luigetti, M. *et al.* SOD1 G93D sporadic amyotrophic lateral sclerosis (SALS) patient with atypical progression and concomitant novel ANG variant. *Neurobiol Aging* **32**, 1924.e15–8 (2011).
- Case, D. A. *et al.* AMBER 10, University of California, San Francisco (2008).

- Jorgensen, W. L., Chandreskar, J., Madura, J. D., Impey, R. W. & Klein, M. L. Comparison of simple potential functions for simulating liquid water. *J. Chem. Phys.* **79**, 926–935 (1983).
- Hornak, V. *et al.* Comparison of multiple Amber force fields and development of improved protein backbone parameters. *Proteins* **65**, 712–725 (2006).
- Berendsen, H. J. C., Postma, J. P. M., van Gunsteren, W. F., Di Nola, A. & Haak, J. R. Molecular dynamics with coupling to an external bath. *J. Chem. Phys.* **81**, 3684–3690 (1984).
- Ryckaert, J. P., Ciccotti, G. & Berendsen, H. J. C. Numerical integration of the cartesian equations of motion of a system with constraints: molecular dynamics of n-alkanes. *Journal of Computational Physics* **23**, 327–341 (1977).
- Essmann, U., Perera, L., Berkowitz, M. L., Darden, T., Lee, H. & Pedersen, L. G. A smooth particle mesh Ewald method. *J Chem Phys* **103**, 8577–8593 (1995).
- DeLano, W. The PyMOL molecular graphics system. <http://www.pymol.org/> Accessed 2013 Jan 14.
- Greenway, M. J. *et al.* ANG mutations segregate with familial and ‘sporadic’ amyotrophic lateral sclerosis. *Nat Genet* **38**, 411–413 (2006).
- van Es, M. A. *et al.* Angiogenin variants in Parkinson disease and amyotrophic lateral sclerosis. *Ann Neurol* **70**, 964–973 (2011).
- van Es, M. A. *et al.* A case of ALS-FTD in a large FALS pedigree with a K171 ANG mutation. *Neurology* **72**, 287–288 (2009).
- Seilhean, D. *et al.* Accumulation of TDP-43 and alpha-actin in an amyotrophic lateral sclerosis patient with the K171 ANG mutation. *Acta Neuropathol* **118**, 561–573 (2009).
- Fernandez-Santiago, R. *et al.* Identification of novel Angiogenin (ANG) gene missense variants in German patients with amyotrophic lateral sclerosis. *J Neurol* **256**, 1337–1342 (2009).
- Paubel, A. *et al.* Mutations of the ANG gene in French patients with sporadic amyotrophic lateral sclerosis. *Arch Neurol* **65**, 1333–1336 (2008).
- Gellera, C. *et al.* Identification of new ANG gene mutations in a large cohort of Italian patients with amyotrophic lateral sclerosis. *Neurogenetics* **9**, 33–40 (2008).
- Conforti, F. L. *et al.* A novel Angiogenin gene mutation in a sporadic patient with amyotrophic lateral sclerosis from southern Italy. *Neuromuscul Disord* **18**, 68–70 (2008).
- Corrado, L. *et al.* Variations in the coding and regulatory sequences of the angiogenin (ANG) gene are not associated to ALS (amyotrophic lateral sclerosis) in the Italian population. *J Neurol Sci* **258**, 123–127 (2007).
- Zou, Z. Y. *et al.* Identification of a novel missense mutation in angiogenin in a Chinese amyotrophic lateral sclerosis cohort. *Amyotroph Lateral Scler* **13**, 270–275 (2012).
- Brown, J. A. *et al.* SOD1, ANG, TARDBP and FUS mutations in amyotrophic lateral sclerosis: a United States clinical testing lab experience. *Amyotroph Lateral Scler* **13**, 217–222 (2012).
- Takahashi, Y. *et al.* Development of a high-throughput microarray-based resequencing system for neurological disorders and its application to molecular genetics of amyotrophic lateral sclerosis. *Arch Neurol* **65**, 1326–1332 (2008).
- Ueki, M. *et al.* Three single nucleotide polymorphisms leading to non-synonymous amino acid substitution in the human ribonuclease 2 and angiogenin genes exhibit markedly less genetic heterogeneity in six populations. *Cell Biochem Funct* **26**, 718–722 (2008).
- van Blitterswijk, M. *et al.* Genetic Overlap between Apparently Sporadic Motor Neuron Diseases. *PLoS One* **7**, e48983 (2012).

Acknowledgements

Programme support for the Supercomputing Facility for Bioinformatics & Computational Biology, Indian Institute of Technology Delhi from the Department of Biotechnology (<http://dbtindia.nic.in/index.asp>), Government of India is gratefully acknowledged.

Author contributions

A.K.P., B.J. and J.G. conceived and designed the experiment. A.K.P. carried out all the experiments including molecular dynamics simulations. A.K.P., B.J. and J.G. analyzed the results and wrote the manuscript. All authors reviewed the manuscript.

Additional information

Supplementary information accompanies this paper at <http://www.nature.com/scientificreports>

Competing financial interests: The authors declare no competing financial interests.

License: This work is licensed under a Creative Commons Attribution-NonCommercial-NoDeriv 3.0 Unported License. To view a copy of this license, visit <http://creativecommons.org/licenses/by-nc-nd/3.0/>

How to cite this article: Padhi, A.K., Jayaram, B. & Gomes, J. Prediction of Functional Loss of Human Angiogenin Mutants Associated with ALS by Molecular Dynamics Simulations. *Sci. Rep.* **3**, 1225; DOI:10.1038/srep01225 (2013).